

## Determination of the fracture energy in polymeric films by *in situ* photoelasticimetry on double edge notch specimen

Florence Dubelley,<sup>1,2,3</sup> Emilie Planes,<sup>1,2</sup> Corine Bas,<sup>1,2</sup> Bernard Yrieix,<sup>3</sup> Lionel Flandin<sup>1,2</sup>

<sup>1</sup>Univ. Savoie Mont Blanc, LEPMI, Chambéry, F-73000, France

<sup>2</sup>CNRS, LEPMI, Grenoble, F-38000, France

<sup>3</sup>EDF R&D, Matériaux Et Mécanique Des Composants, Site Des Renardières, Moret-sur-Loing, 77818, France

Correspondence to: E. Planes (E-mail: Emilie.planes@univ-smb.fr)

**ABSTRACT:** The fracture toughness is key parameters to select polymeric films. The essential work of fracture (EWF) is a phenomenological but efficient way to characterize this resistance to fracture. One can gain valuable information on the resistance to perforation and propagation of flaws. A new technique was developed to better understanding the EWF experiments. A tensile test combined to photoelasticimetry allows following *in situ* the geometry and amount of plastic deformation on double edge notched specimen. The EWF parameters are determined when the plastic deformation appears constant, so when the fracture energy  $W_f$  only contributes to rupture filament. This new methodology requires just a single sample, whereas at least five specimens are required for general method. It will help characterize expensive polymeric films or reveal the heterogeneous behavior, for instance after polymer ageing. © 2015 Wiley Periodicals, Inc. *J. Appl. Polym. Sci.* **2016**, *133*, 42854.

**KEYWORDS:** mechanical properties; optical properties; polyolefins

Received 27 May 2015; accepted 24 August 2015

DOI: 10.1002/app.42854

### INTRODUCTION

Polymers are a part of everyday life as they are used in a wide variety of applications. Their fracture toughness is often a key parameter when used as films or membranes, where a small flaw may result in the loss of these key properties. This is especially the case in food packaging, or any of the numerous applications where the polymer is used as a barrier. The perforation and the tearing of the film, consisting of several layers of polymers, lead to the loss of barrier properties – gas and water vapor – and therefore the protection of the food.

Damage phenomena result either from design or construction error (assembly, manufacture, transportation ...) or ageing of the polymer. The tensile strength of materials is commonly used as a parameter to estimate their resistance to tearing.

In the literature related to fracture mechanics, more distinctive methods of analysis are proposed. In the case of thin films, the essential work of fracture (EWF) method is usually preferred.<sup>1–7</sup> This technique presents a straightforward specimen's preparation and easy testing procedure. It furnishes meaningful results on parameters otherwise difficult to obtain. EWF method enables to determine both the energy used to propagate a crack (specific essential work of fracture  $w_e$ ) and that dissipated in a plastic deformation process ( $\beta w_p$ ).

Various authors brought to light relationships between the physico-chemical properties of the polymeric film and the mechanical properties from the EWF method. For instance, Garnier *et al.*<sup>8</sup> and Vu *et al.*<sup>9</sup> showed the influence of the crystallinity of PET on  $w_e$ . Moukheiber *et al.*<sup>10</sup> studied the influence of the chain length and ionic exchange capacity (IEC) of Nafion-like structures on EWF parameters for membranes used in fuel cells. Barany *et al.*<sup>11</sup> and several other<sup>7,12</sup> tested the resistance to tearing of polymeric films after hydrothermal aging (100%HR, 60°C). Barany showed it induces spectacular changes in PET: the essential work of fracture  $w_e$  is divided by 12, while  $\beta w_p$  dropped by a ratio of 0.3. This series of experiments mean that the perforation becomes much easier after aging. This will jeopardize the final product. In comparison, more conventional mechanical properties such as Young's modulus or even elongation at break failed to reveal the changes within the polymer induced by aging. The strong discrepancy between the experimental results also means that the tensile tests are not appropriate to probe this kind of damage.

Unfortunately, the EWF method requires the use of at least five samples of the same kind in order to vary the initial length of the filament. Getting a homogeneous series of samples is often not compatible with the study of polymer aging. This is expensive, time consuming, and most of all strong heterogeneities

may result from the aging step. We propose here a new technique from which the same amount of information may be obtained with a single sample. The latter method was first obtained by coupling of photoelasticity and tensile test on notched specimen. The photoelasticity was employed to observe, by birefringence, the rupture propagation and the area altered by the stress at every moment of the test. Various authors have already used the photoelasticity to observe their samples without linking their comments directly to the EWF parameters.<sup>10,13,14</sup> To implement this method, the used polymer film has to be transparent, birefringent under mechanical stress, thin, and ductile to meet different criteria for applying EWF method. The Polyethylene (PE) seems to be a good candidate and has already been the subject of many studies.<sup>2,4,14–21</sup>

## EXPERIMENTAL

### Material

The base film is a Low Density Polyethylene (LDPE) film of 40  $\mu\text{m}$  in thickness. This is a semi-crystalline polymer with about 34 wt % crystallinity as measured by DSC.

### Tensile Test

Tensile tests were performed on standard dumb-bell shape specimens with a 12 mm gauge length  $L_0$  and 2 mm width (ISO527 sample-test B2) at room temperature ( $(23 \pm 1)^\circ\text{C}$ ) on an ADAMEL Lhomargy tensile machine (100 N) with a cross-head speed of 5 mm  $\text{min}^{-1}$ .

Tensile tests were carried out in two loading directions: in machine (MD) and transverse (TD) directions. For each direction, five specimens were tested.

The data were plotted in a true stress  $\sigma_H$  versus true strain  $\varepsilon_H$ , which were obtained assuming a constant volume of the specimens during deformation:<sup>22</sup>

$$\sigma_H = \frac{F}{S_0} \left( 1 + \frac{\Delta L}{L_0} \right) \quad (1)$$

$$\varepsilon_H = \ln \left( 1 + \frac{\Delta L}{L_0} \right) \quad (2)$$

with  $F$  the Load (N),  $S_0$  the initial surface ( $\text{m}^2$ ) on which the force is applied and  $\Delta L$  is elongation (m).

### Essential Work of Fracture

The Double-Edge Notched Tension (DENT) method was first developed by Broberg<sup>23–25</sup> for characterizing fracture resistance. It was then extended by Cotterell and Reddel<sup>26</sup> to the current concept of essential work of fracture to metal sheets, before extending to polymers.<sup>5</sup>

The fundamental concept of the EWF method is based on the energy partition, which separates the total fracture energy into two components:

$$W_f = W_e + W_p \quad (3)$$

$W_e$ , the essential work of fracture (J), represents the energy dissipated in the inner fracture process zone (IFPZ), where the tearing process occurs.  $W_e$  can be interpreted as the work required to create two new surfaces. This work is used initially

to form a necking at the crack-tip and then to tear this necking.  $W_p$ , the non-essential work of fracture (J), represents the energy dissipated in the outer plastic deformation zone (OPDZ), where the plastic deformation and heat dissipative process occur.

The essential work of fracture  $W_e$  is proportional to the ligament length  $L$  and the non-essential work of fracture  $W_p$  is dimensionally proportional to a surface  $L^2$  as represented in the following equation:

$$W_f = w_e L t + \beta w_p t L^2 \quad (4)$$

with  $w_e$  the specific essential work of fracture ( $\text{kJ m}^{-2}$ ),  $w_p$  the specific non-essential work of fracture ( $\text{MJ m}^{-3}$ ),  $L$  the ligament length (m),  $t$  the thickness of sample (m), and  $\beta$  a shape factor related to the shape of the plastic zone.

By referring all terms to the unit surface, the following equation is obtained:

$$w_f = \frac{W_f}{L t} = w_e + \beta w_p L \quad (5)$$

with  $w_f$  specific work of fracture ( $\text{kJ m}^{-2}$ ).

According to this equation, a linear relationship is founded between  $L$  and  $w_f$ .  $w_e$  can be obtained by extrapolating  $w_f$  versus  $L$  line to  $L=0$ , considered as fracture toughness, and  $\beta w_p$  can be obtained from the slope of the curve.  $w_f$  versus  $L$  curve is carry out by conducting DENT tests for different ligament lengths.

This test is to be performed in plane-stress conditions. The ligament length  $L$  must thus be larger than 3–5 times the sample's thickness and smaller than the third of its width. In this condition, the plastic deformation occurs within the ligament section and the edge effects are attenuated. For plane stress conditions, two other requirements should be met<sup>1,5,27</sup>: full ligament yielding prior to crack initiation and self-similar load-displacement curves.

For the measurement, DENT specimens used in the present study were cut from rectangular shape (length: 50 mm and width: 25 mm) in the Machine Direction (MD) and Transverse Direction (TD), Figure 1. The length of the ligament  $L$ , ranging from 2 to 8 mm, was measured precisely using an optical microscope MICRO.VU VERTEX. The specimens were loaded on an ADAMEL Lhomargy tensile machine (100 N) at a cross-head speed of 5 mm  $\text{min}^{-1}$ .

### Photoelasticity

Photoelasticity is a technique based on the optical birefringence induced by the application of a stress. The material, optically isotropic at rest (optical index  $n_0$ ), becomes anisotropic when is subjected to mechanical loading. This phenomenon was first reported by Brewster in the 19<sup>th</sup> century. The change in indices was thoroughly linked to the main strains by Maxwell and Neumann.<sup>28</sup>

Photoelasticity bench consist of a circular polariscope. This polariscope includes a light source (white), a polarizer, and an analyzer (that is crossed with respect to the polarizer), two quarter-wave-plates inserted between polaroids. These quarter-wave-plates positioned at  $90^\circ$  to each other and their optical axes are at  $45^\circ$  to those of the analyzer and polarizer. They allow

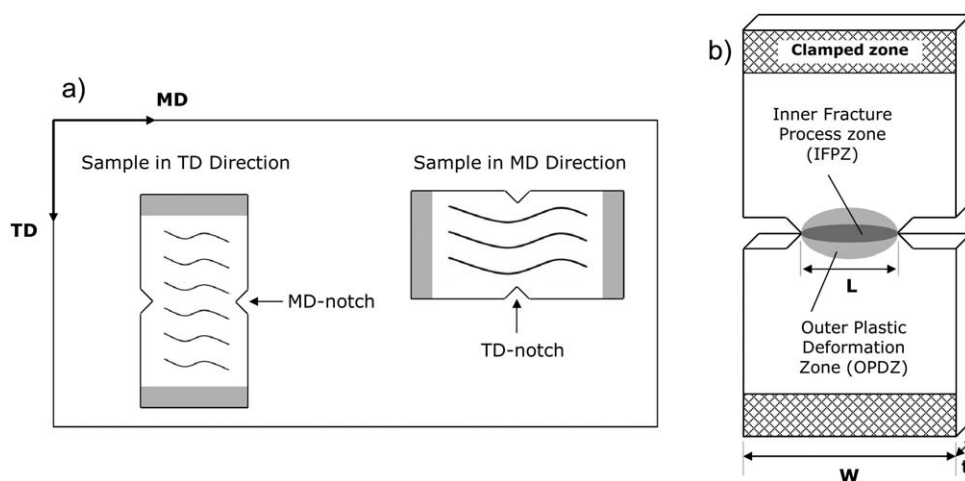


**Figure 1.** (a) Definition of MD and TD direction and (b) DENT geometry showing the process (IFPZ) and the plastic zone (OPDZ).

to get rid of the isochromes and to observe shamelessly isochromatics. A camera was used to record (one photography per second) the birefringence development of the DENT and dumb bell shape specimens, crack propagation and the size of the plastic zone. At analyzer output, the intensity of light conforms to the following equation:<sup>28</sup>

$$I = A \sin^2 \left( \frac{\pi C d}{\lambda} (\sigma_1 - \sigma_2) \right) \quad (6)$$

with  $I$  the Intensity,  $A$  a constant,  $C$  the stress optical coefficient (Brewster,  $1 \text{ Br} = 10^{-12} \text{ m}^2 \text{ N}^{-1}$ ),  $\lambda$  the wavelength ( $\text{cm}^{-1}$ ), and  $d$  the sample thickness (m).

Under white light, each color ( $\lambda$ ) extinguishes at a different value of  $(\sigma_1 - \sigma_2)$  and is then observed complementary color fringes in sample:

$$I=0 \quad \sin^2 \left( \frac{\pi C d}{\lambda} (\sigma_1 - \sigma_2) \right) = 0 \quad \frac{C d}{\lambda} (\sigma_1 - \sigma_2) = N \quad (7)$$

with  $N$  the order of fringe. The Michel Levy Color Chart allows a fairly objective assessment of the observed color and of the corresponding optical delay ( $\delta = N\lambda$ ).<sup>29</sup>

## RESULTS AND DISCUSSION

### Optical Stress Coefficient

Prior to EWF test, tensile tests were performed on the PE in order to determine the stress optical coefficient  $C$ . A high value of  $C$  helps the observation of birefringence on the sample. The tensile curves (true stress versus true strain) are presented in Figure 2 for both directions, MD and TD. The slight anisotropy of PE is visible.

In photoelasticimetry, the isochrones order is the most reliable way to first identify the main constraints. For each color an optical delay  $\delta = N\lambda$  is associated to a change of one order. In addition, eq. (7) in tensile test simply becomes:

$$C = \frac{\delta}{d_0 \sigma_1} \quad (8)$$

The coefficient  $C$  then determined by knowing that for each color  $\sigma_1$  matches an optical delay  $\delta$ . The optical stress coeffi-

icients in both directions (TD and MD) are sufficient to observe photoelasticimetry in PE even at low stresses. The optical delay for transition order 1 to order 2 was chosen (from purple to violet). The correlation between image analysis and  $\sigma_H - \varepsilon_H$  curve furnished  $\sigma_1$  and  $C$ . The stress optical coefficients in TD and MD direction are respectively  $(1093 \pm 29) \text{ Br}$  in TD direction and  $(916 \pm 45) \text{ Br}$  in MD direction, after thickness correction (constant volume). These values are in agreement with the ones proposed in the literature for PE by Koyama *et al.* ( $1300 \text{ Br}$ ).<sup>30</sup> Other authors evaluated the same coefficient to be in the range  $1200\text{--}2200 \text{ Br}$ .<sup>30,31</sup>

### Classic EWF Method

Figure 3 displays the load-displacement curve of DENT specimens with various ligament lengths in both directions (MD and TD). The maximum load and extension at rupture increased as expected with ligament's length. A similar shape

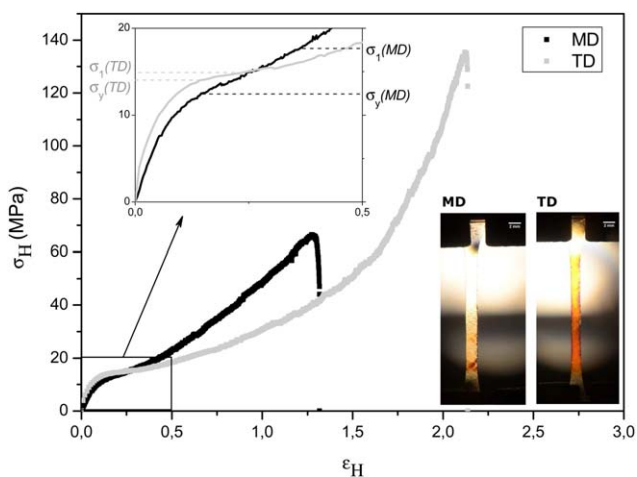


**Figure 2.** Typical true stress–true strain curves of PE samples under tensile test in MD and TD directions with photoelastic observation at  $\sigma_1$ . [Color figure can be viewed in the online issue, which is available at [wileyonlinelibrary.com](http://wileyonlinelibrary.com).]

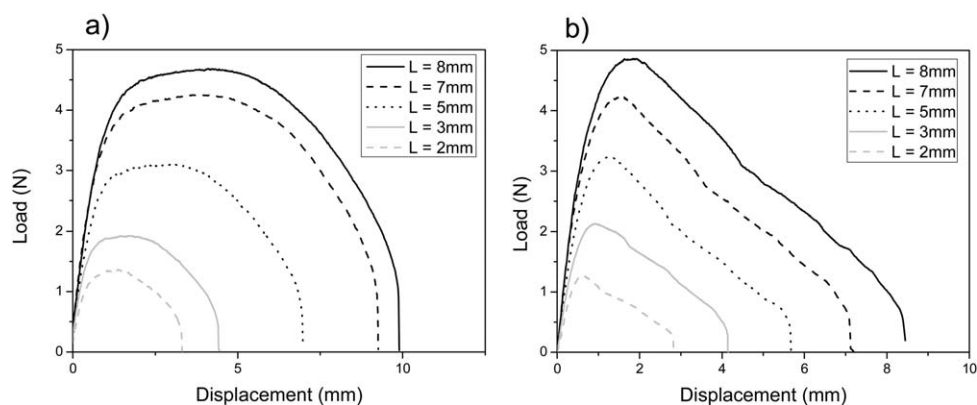


**Figure 3.** Load-displacement curves of DENT specimens of PE (a) in MD direction, (b) in TD direction.

of load-displacement curve was observed for all measured lengths for each direction. This is typical for good EWF conditions.

Figure 4 presents the load-displacement curve superposed with the ligament length, as measured by image analysis during the DENT test versus displacement for the PE with 7 mm initial ligament length in MD direction. The same curves for the PE with 7 mm initial ligament length in TD direction are plotted in Figure 5.

In both directions (MD and TD), the crack propagation, as revealed by image analysis, takes place slightly before the polymer yields. In other words, the ligament is not in complete yielding before the propagation. The last criterion for properly applying the EWF method is not met.

Many experimental studies using the EWF concepts<sup>1,10,32,33</sup> were however performed on polymeric systems in the same conditions, as noticed by Barany *et al.*<sup>1</sup> It seems actually reasonable to assume that the similarity in load-displacement curves and plane-stress conditions are the only real prerequisites to the appropriate application of the EWF method.

This was further validated in Figure 6 that depicts the essential work of fracture as a function of the ligament length for PE in both notch directions (MD and TD). A linear correlation is evidenced, as theoretically expected. Very large  $R^2$  coefficients (0.997 and 0.986 in MD and TD, respectively) are found, even with a large range of initial length. Williams and Rink proposed that this value should be above 0.98 for EWF analysis.<sup>34</sup>

$w_e$  and  $\beta w_p$  are summarized in Table I. Casellas *et al.*<sup>21</sup> studied a similar LDPE in similar conditions. Their results, reported in Figure 6, are in very good agreement with our data in the TD direction. The authors did however not present the anisotropy of their materials in their publication.

In Figure 6, a small anisotropy of the polymer in tensile test was observed, Table I. The difference between MD and TD is significantly more noticeable in the values of the specific essential work of fracture  $w_e$  and the non-essential work of fracture  $\beta w_p$ . The TD-notch (crack propagates in TD direction) appeared tougher than the MD-notch. These results are likely to result from the polymeric chains, preferentially oriented in MD direction as show in Figure 1(a). The covalent bounds in the

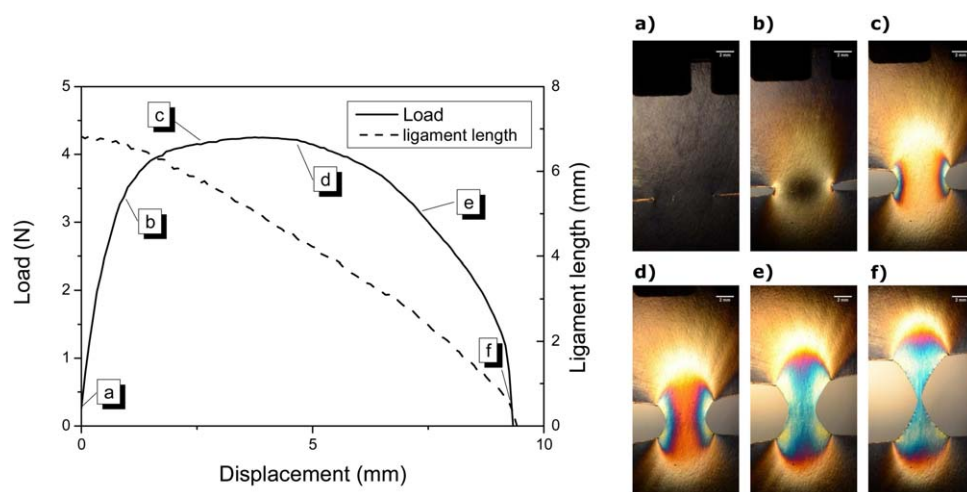


**Figure 4.** Load-displacement curve and propagation of fracture of ligament length  $L=7$  mm in MD direction with (a–f) the different stages of plastic zone development/crack propagation. [Color figure can be viewed in the online issue, which is available at [wileyonlinelibrary.com](http://wileyonlinelibrary.com).]

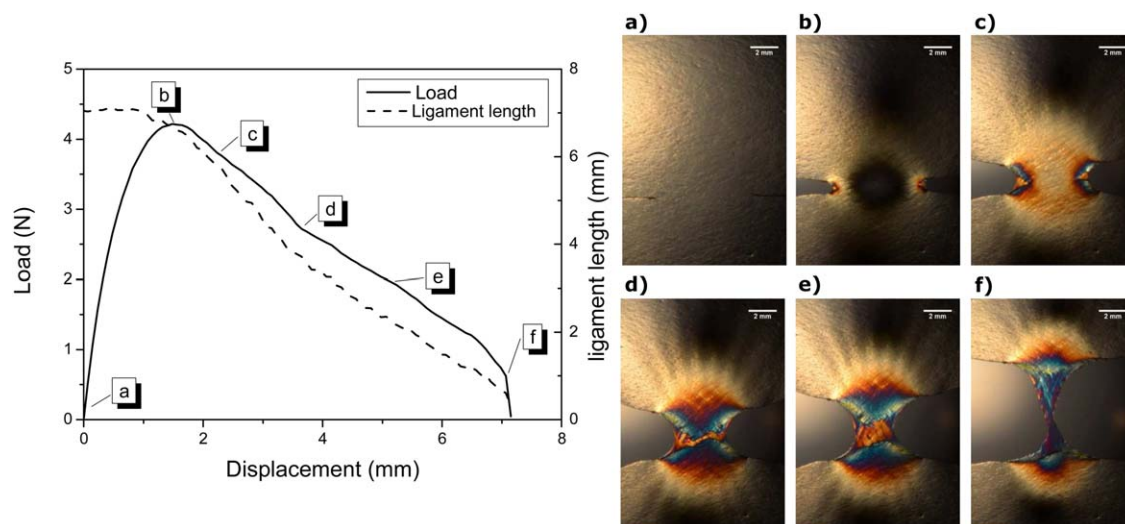


**Figure 5.** Load-displacement curve and propagation of fracture of ligament length  $L=7$  mm in TD direction with (a–f) the different stages of plastic zone development/crack propagation. [Color figure can be viewed in the online issue, which is available at [wileyonlinelibrary.com](http://wileyonlinelibrary.com).]

polymer chains prevent the initiation and propagation of the defects. This observation is in agreement with that of Lee *et al.* on polyethylene film of  $30 \mu\text{m}$  in thickness.<sup>14</sup>

#### New EWF Method: With One Sample

In eq. (4),  $L$  is the initial length of the ligament and  $W_f$  is the total energy required to break the entire ligament length  $L$ . As the physical model for the J analysis of the tearing of ductile polymers, it was assumed that the crack propagation was independent of the crack growth history.<sup>35</sup> Consequently we can consider that this length  $L$  may also be viewed as a continuous sum of small ligaments  $l$ , which can break gradually and independently from each other. It is possible to substitute in the previous equation the total ligament length  $L$  by  $l$ , the change in ligament length at some time  $\tau$ . As a result,  $W_f$  depends on the length  $l$ , noted  $W_f[l]$ , and corresponds to the energy necessary to break the length left on the ligament  $l$ :

$$W_f(l) = w_e l t + l^2 t \beta w_p \quad (9)$$

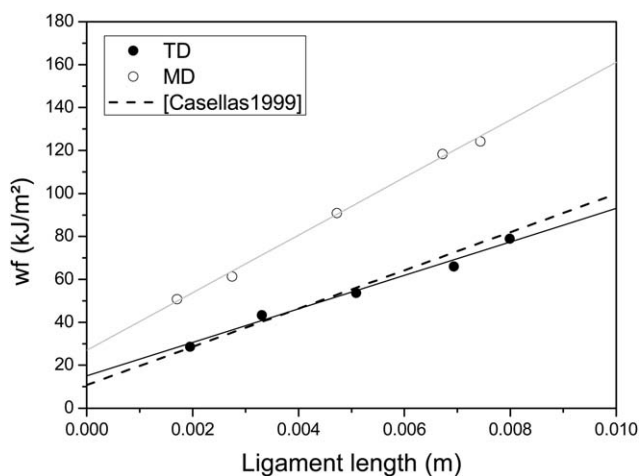
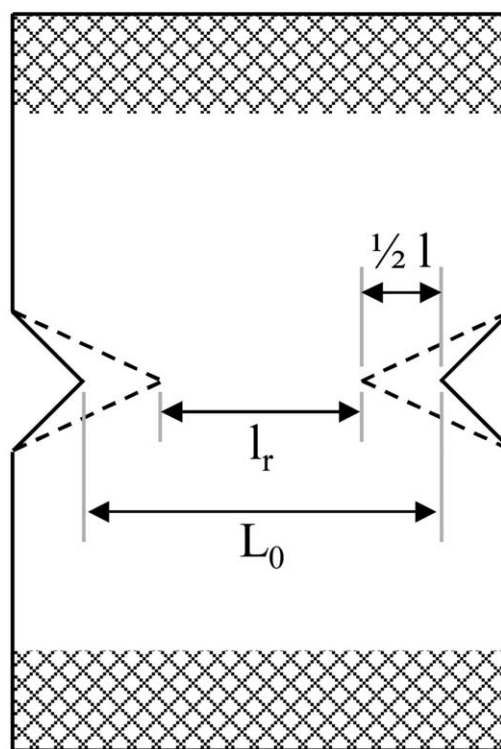


**Figure 6.** Relationship between the specific work of fracture and the ligament length under EWF test.

**Table I.** Calculated EWF Parameters

	$w_e$ ( $\text{kJ m}^{-2}$ )	$\beta w_p$ ( $\text{MJ m}^{-3}$ )
MD	$27 \pm 2$	$13.4 \pm 0.4$
TD	$15 \pm 3$	$7.8 \pm 0.5$



—  $t_0$  : initial state  
 ---  $t_0+dt$ : after loading  $dF$

**Figure 7.** Definition of the different ligament lengths during the test.

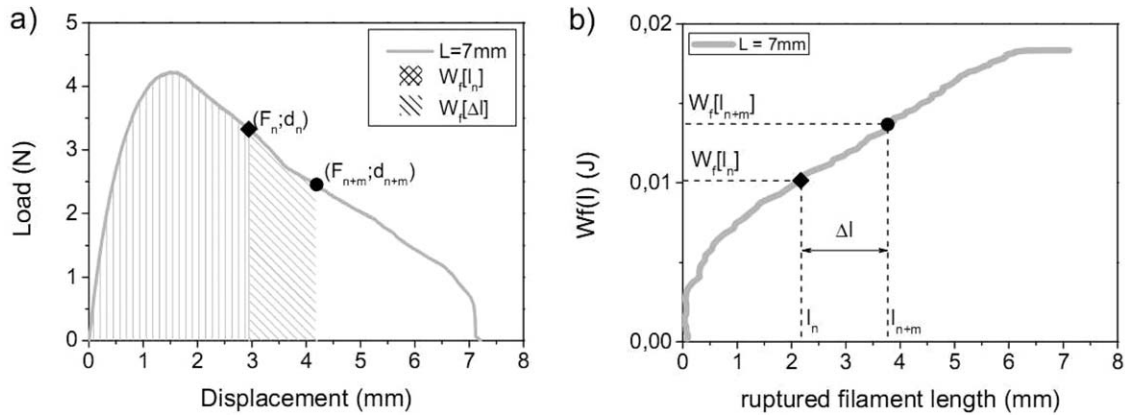


**Figure 8.** (a) Load-displacement curve of DENT specimen with  $L=7$  mm in MD direction and (b) Energy  $W_f$  required to gradually break the ligament  $l$ .

In this equation, it is possible to distinguish the elastic and plastic energy generated with the increase of the ligament length  $l$ .

A careful image analysis was used to determine accurately the length of the remaining ligament  $l_r$  as a function of time  $\tau$  (and thus for a given displacement). Knowing the initial length  $L$  of the ligament, the length of the broken ligament is defined by:

$$l = L - l_r \quad (10)$$

Figure 7 summarizes the different lengths of the ligament during the test.

The energy  $W_f[l]$  is determined using the raw load-displacement curve. The energy required to break a length  $l_n$  is given by the integration of the raw data up to a crosshead displacement  $d_n$ .  $W_f[l_n]$  indeed corresponds to the area under the load-displacement curve to the point of coordinates  $(F_n; d_n)$ . The next displacement  $\Delta d$  of the crosshead causes a rupture  $\Delta l$  of ligament and the corresponding energy is  $W_f[\Delta l]$ , Figure 8(a). The energy to break  $l_{n+m} = \Delta l + l_n$  becomes:

$$W_f(l_{n+m}) = W_f(l_n) + W_f(\Delta l) \quad (11)$$

This is resumed until complete rupture of the ligament. With this stepwise method, one can directly measure, with a single run, the energy  $W_f[l]$  required to gradually break the ligament, as a function of the amount of ruptured film. This incremental approach is summarized in Figure 8. As explained previously with the eq. (9) this fracture energy  $W_f$  can be elastic and plastic.

$W_f[l]$  curve has a parabolic shape, as expected with eq. (9). On  $W_f[L]$  curve, Figure 9, three regimes are identified:

1. Plain stress/strain transition;
2. Plane stress uncontained yield;
3. Plane stress contained yield.

$w_e$  and  $w_p$  should be measured in pure plane stress state independently from the energy used to yielding the film. This may be easily identified in the  $W_f[l]-l$  curve, Figure 8(b), to obtain  $w_e$  and  $w_p$  with the new method.

**Measurements of the Shape Factor.** The shape factor  $\beta$  is linked to the OPDZ geometry. The OPDZ is sometimes observable in post-mortem samples.<sup>1,11,36</sup> Martinez *et al.* exhibit in their work the shape factor by using the relation between  $h$  (plastic zone height) and  $l$  for different possibilities for the plastic zone shape,<sup>37</sup> Figure 10.

In the present work with PE, the plastic area is not visible on post-mortem samples. In contrast, photoelasticimetry characterization may be advantageously used to dynamically and accurately measure the OPDZ and determine its shape factor. Photoelastic observations of OPDZ in TD and MD directions are given respectively in Figure 11. The selected areas correspond to frontier between areas where the stress is above and below the yield stress of the polymer as determined by tensile tests.

For the test in MD direction, the determination of the shape factor is possible by a straightforward identification of  $h$  and  $l$  parameters. On the other hand, for the test in TD direction, estimating the value of  $h$  is more difficult. In addition, the shape of OPDZ changes with time with both kinds of sample. The determination of the actual OPDZ area was thus preferred. The limit of the measurement of OPDZ area is considered as the transition of order 1 to order 2 ( $\delta = 575 \times 10^{-9}$  m). Macroscopically it is characterized by a transition from purple to

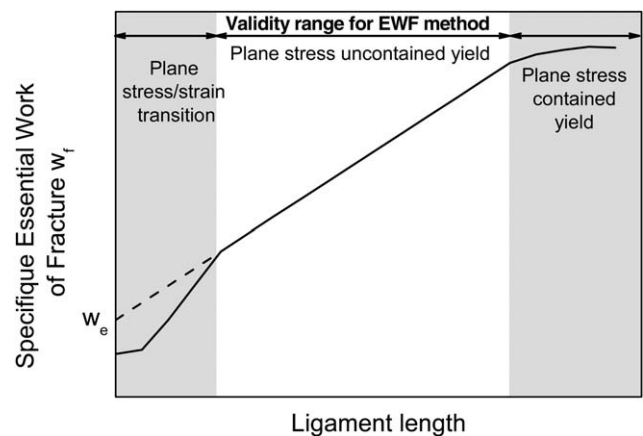


**Figure 9.** Schematic variation of the specific work fracture with ligament length.

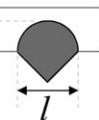
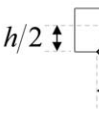
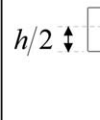
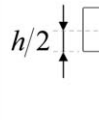
	Circle	Diamond	Ellipse	Parabolic
Geometry				
$\beta$ value	$\beta = \frac{\pi}{4}$	$\beta = \frac{\pi h}{2l}$	$\beta = \frac{\pi h}{4l}$	$\beta = \frac{h}{kl}$

Figure 10. OPDZ geometry and relationship with the parameter.

violet from Michel Levy Color Chart. This method was preferred because it seemed not subjective. In addition, the true stress  $\sigma_H$  to  $\delta = 575 \times 10^{-9}$  m was found equal to 14.50 MPa, very close to the true stress at the yield of  $14.1 \pm 0.5$  MPa in TD direction, Figure 2. The transition purple to violet can thus be used to designate the limit for OPDZ.

These measurements were performed for each direction and ligament length thanks to a meticulous image analysis. The results in Figure 12 reveal that the OPDZ area initially increases with

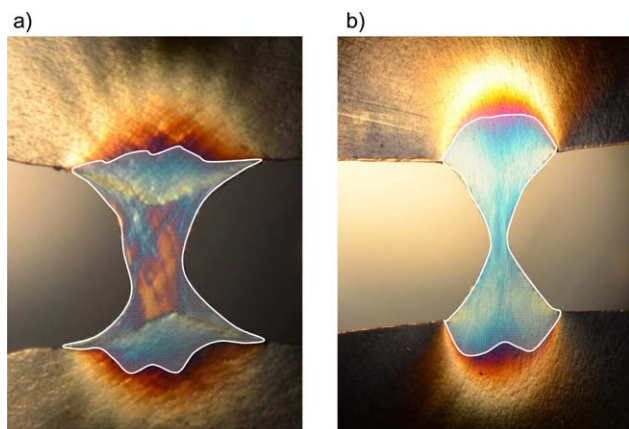


Figure 11. Photoelastic observation of crack propagation and OPDZ (a) in TD direction and (b) in MD direction. [Color figure can be viewed in the online issue, which is available at wileyonlinelibrary.com.]

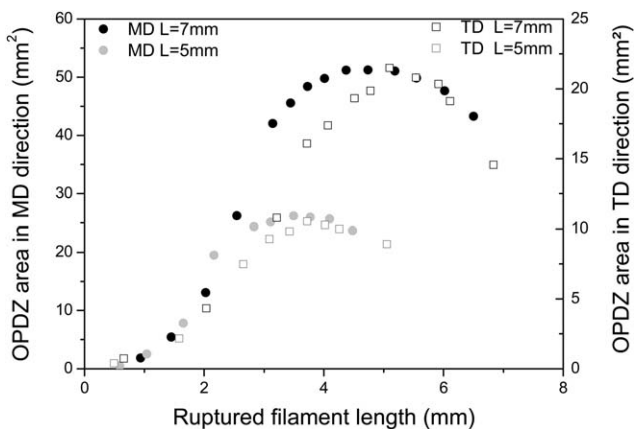


Figure 12. OPDZ areas of DENT PE versus rupture filament length  $l$  with  $L = 7$  mm and 5 mm in MD and TD directions.

the rupture of the ligament. This expected behavior indicates that the ductile films accommodate the stress localization to prevent rupture in the DENT sample. On the sample with initially 7 mm of filament, a plateau is reached where the amount of plastic deformation is somewhat constant after about 3 mm of filament rupture. At the end of the test, the measured amount of OPDZ decreases. These observations are in good agreement with the results from Lee *et al.*,<sup>14</sup> who performed similar measurements on PE films with 30  $\mu\text{m}$  in thickness.

From these observations, it was possible to assume that when the OPDZ area appeared constant, the sole contribution of  $W_f$  was a specific energy to break the filament. This is thus directly associated to  $W_e$ .

**Identification of EWF Parameters.** Quite interestingly, the curve  $W_f[l]$  presents a linear behavior in the constant OPDZ area regime, Figure 13. Following the method commonly used for EWF tests, the intersection of the straight line  $W_f[l]$  (in OPDZ area constant) with the y-axis is defined as the fracture energy  $W_e$  in Figure 13. The specific fracture energy  $w_e$  is then deduced by dividing  $W_e$  by the total surface broken ( $tL$ ).

The  $\beta w_p$  parameter may be determined using eq. (12), directly derived from the eq. (5):

$$\beta w_p = \frac{w_f - w_e}{L} \quad (12)$$

Figure 14 presents the extracted EWF parameters obtained with our samples for MD and TD directions.  $w_e$  and  $\beta w_p$  values were

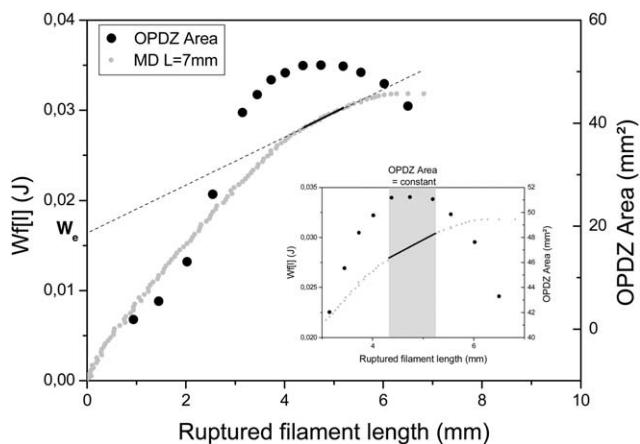


Figure 13. Determination of the plane stress state contained yield on  $W_f[l]-l$  curve with the constant OPDZ area.

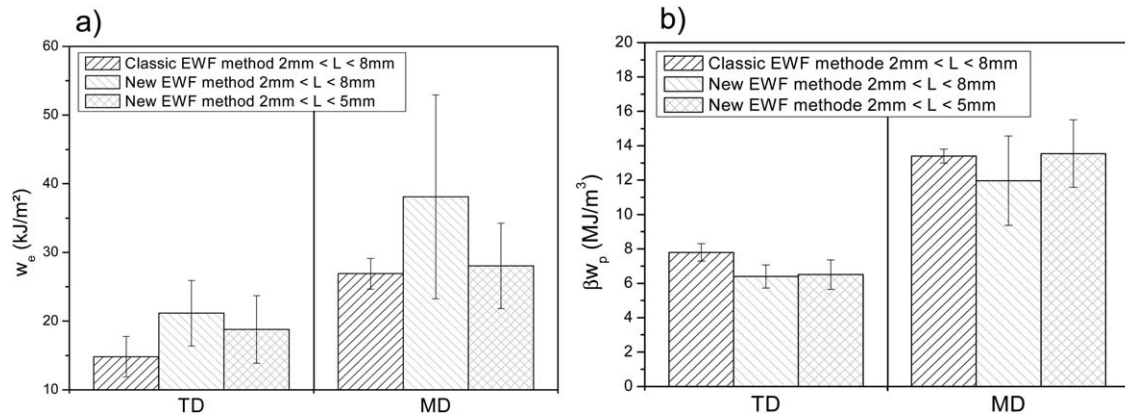


Figure 14. Comparison of EWF parameters calculated between the two methods.

plotted both from conventional EWF tests and from the method described in the present work. In the latter case,  $w_e$  was averaged for all ligament lengths. As a result, the error bars for  $w_e$  are rather large, especially in MD direction.

To try and understand where this scatter came from, the  $w_e$  values were plotted individually as a function of the ligaments length in Figure 15. The values of  $w_e$  very close to the ones obtained with the regular EWF test for short filament gradually deviate for longer values, and especially for  $L=7$  mm.

This result demonstrates that the length of the ligament must be chosen sufficiently small as compared to the total width of the sample. This hypothesis was already made in the EWF tests in order to contain the plastic deformation at the section of the ligament. It is usually accepted that the length of the filament should not exceed one-third of the sample's width.<sup>1</sup> Although this requirement mathematically fulfilled with our sample with ligaments of 7 mm and 8 mm the current measurements clearly show that the plastic surface may be extended outside of the ligament, which causes an over-estimation of  $w_e$ . In other words, the geometrical requirements on the EWF methods should be reinforced with our systems.

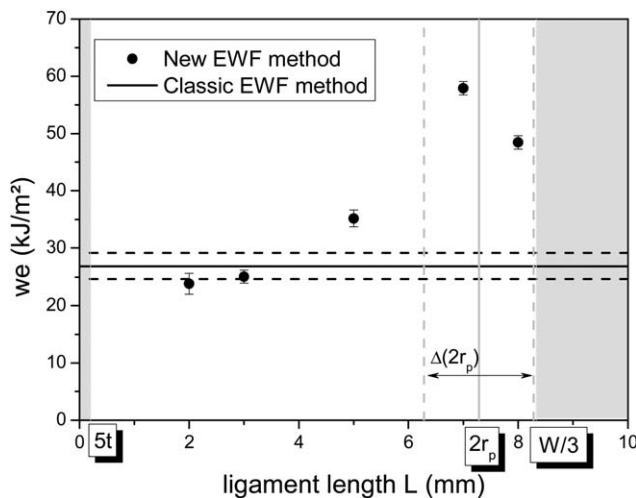


Figure 15. Specific essential work of fracture of DENT specimen in MD direction for different ligaments length.

Defining the size of the plastic zone as  $2r_p$  (this definition was also classically applied for numerous polymer films, as for example polyethylene,<sup>20</sup> another upper limit for the length of the ligament for the proper application of the EWF method should be verified. The value of  $2r_p$  is given by the following equation:<sup>6,20</sup>

$$2r_p = \frac{1}{\pi} \frac{E w_e}{\sigma_y^2} \quad (13)$$

with  $E$  the Young's Modulus (Pa).  $E$  was measured with the tensile test showed above, and was close to 160 MPa for the MD direction. Following eq. (13),  $2r_p$  would become 7.3 mm. With the uncertainty on  $w_e$  and other parameters, the ligament length 7 mm can be considered out of validity range, Figure 15. The parameters  $w_e$  and  $\beta w_p$  determined by disregarding the 7 mm and 8 mm ligaments length are in good agreement with the ones derived from the regular EWF method, Figure 14.

## CONCLUSIONS

A new technique was developed to better understanding the EWF experiments. It revealed a narrow window in ligament length where the method may be applied rigorously, i.e. following the mechanical hypotheses. Experimentally, the estimation of  $w_e$  and  $\beta w_p$  parameters remains satisfactory in a much broader range of filament length. It suggests that the initial hypotheses for the Cotterell test may be too demanding. The coupled measurements proposed in this study permitted to determine  $w_e$  and  $\beta w_p$  with a single sample. The only limitation of this new method is that its rigorous application requires a material that becomes birefringent under constraints. A tensile test coupled to photoelasticimetry may first be used to determine the stress optical coefficient of the materials. The choice of the right ligament length  $L$  is essential to obtain reliable results. It must be in the validity range of  $5t < L < (2r_p W/3)$ . The coupled measurements showed that one should preferentially use a ligament length as far from these limits as possible. If  $L$  is close to  $5t$ , OPDZ area is small and difficult to observe accurately. In contrast, if  $L$  is close to  $W/3$ ,  $w_e$  may be overestimated.  $L=5$  mm seems to be a good compromise in our case. The series of measurements shed some new light on the EWF testing method and will now be very useful to determine the resistance to crack propagation with very little amount of material. We believe it



will be especially helpful for expensive or hard to process polymeric films or to characterize the heterogeneous behavior of films, for instance after ageing.

#### ACKNOWLEDGMENTS

The authors acknowledge the ANR (French National Research Agency) for his financial support of the EMMA-PIV projects. This work was performed within the framework of the center of Excellence of Multifunctional Architected Materials (CEMAM) n°AN-10-LABX-44-01. Special thanks are also given to Pauline Ratel and Nicolas Crowin for their assistance and numerous hours to perform experimental work.

#### REFERENCES

1. Barany, T.; Czigany, T.; Karger-Kocsis, J. *Prog. Polym. Sci.* **2010**, *35*, 1257.
2. Wu, J.; Mai, Y. W. *Polym. Eng. Sci.* **1996**, *36*, 2275.
3. Saleemi, A. S.; Nairn, J. A. *Polym. Eng. Sci.* **1990**, *30*, 211.
4. Mai, Y. W.; Powell, P. J. *Polym. Sci. Part B: Polym. Phys.* **1991**, *29*, 785.
5. Mai, Y. W.; Cotterell, B. *Int. J. Fract.* **1986**, *32*, 105.
6. Karger-Kocsis, J.; Czigany, T. *Polymer* **1996**, *37*, 2433.
7. Barany, T.; Foldes, E.; Czigany, T. *Express Polymer. Lett.* **2007**, *1*, 180.
8. Garnier, G.; Chehab, B.; Yrieix, B.; Brechet, Y.; Flandin, L. *J. Mater. Sci.* **2009**, *44*, 5537.
9. Vu, H. N.; Gauthier, C.; Lame, O.; Cavaillé, J. Y. *Polym. Int.* **2012**, *61*, 1094.
10. Moukheiber, E.; Bas, C.; Flandin, L. *Int. J. Hydrogen Energy* **2014**, *39*, 2717.
11. Barany, T.; Karger-Kocsis, J.; Czigany, T. *Polym. Degrad. Stab.* **2003**, *82*, 271.
12. Ho, C. H.; Vu-Khanh, T. *Theor. Appl. Fract. Mech.* **2004**, *41*, 103.
13. Light, M. E.; Lesser, A. J. *J. Mater. Sci.* **2005**, *40*, 2861.
14. Lee, C. H.; Sue, H. J.; Fiscus, D. M. *Polym. Test* **2013**, *32*, 256.
15. Peres, F. M.; Shön, C. G. *J. Mater. Sci.* **2008**, *43*, 1844.
16. Pegoretti, A.; Castellani, L.; Franchini, L.; Mariani, P.; Penati, A. *Eng. Fract. Mech.* **2009**, *76*, 2788.
17. Na, B.; Lv, R. *J. Polym. Sci. Part B: Polym. Phys.* **2006**, *44*, 2880.
18. Mai, Y. W.; Cotterell, B.; Horlyck, R.; Vigna, G. *Polym. Eng. Sci.* **1987**, *27*, 804.
19. Kwon, H. J.; Jar, P. Y. B. *Polym. Eng. Sci.* **2007**, *47*, 1327.
20. Chan, W. Y. F.; Williams, J. G. *Polymer* **1994**, *35*, 1666.
21. Casellas, J. J.; Frontini, P. M.; Carella, J. M. *J. Appl. Polym. Sci.* **1999**, *74*, 781.
22. G'sell, C.; Jonas, J. J. *J. Mater. Sci.* **1979**, *14*, 583.
23. Broberg, K. B. *J. Mech. Phys. Solids* **1975**, *23*, 215.
24. Broberg, K. B. *J. Mech. Phys. Solids* **1971**, *19*, 407.
25. Broberg, K. B. *Int. J. Fract. Mech.* **1968**, *4*, 11.
26. Cotterell, B.; Reddel, J. K. *Int. J. Fract.* **1977**, *13*, 267.
27. Cotterell, B.; Pardoën, T.; Atkins, A. G. *Eng. Fract. Mech.* **2005**, *72*, 827.
28. Brémand, F.; Cotttron, M.; Doumalin, P.; Dupré, J. C.; Germaneau, A.; Valle, V. *Techniques De L'ingénieur* **2011**, R1850v2, 1.
29. M. Magnus, Michel-Lévy Color Chart. Identification of Minerals in Polarized Light. Technical Report, Carl Zeiss Microlmaging GmbH TU Bergakademie Freiberg – Institute of Geology and Paleontology, **2011**.
30. Koyama, K.; Ishizuka, O. *J. Polym. Sci. Part B: Polym. Phys.* **1989**, *27*, 297.
31. Gortemaker, F. H.; Hansen, M. G.; de Cindio, B.; Janeschitz-Kriegl, H. *Rheol. Acta.* **1976**, *15*, 242.
32. MasPOCH, M. Ll.; Hénault, V.; Ferrer-Balas, D.; Velasco, J. I.; Santana, O. O. *Polym. Test* **2000**, *19*, 559.
33. Karger-Kocsis, J. *Polym. Bull.* **1996**, *37*, 119.
34. Williams, J. G.; Rink, M. *Eng. Fract. Mech.* **2007**, *74*, 1009.
35. Hodgkinson, J. M.; Williams, J. G. *J. Mater. Sci.* **1981**, *16*, 50.
36. Zhao, H.; Li, R. K. Y. *Mech. Mater.* **2006**, *38*, 100.
37. Martinez, A. B.; Gamez-Perez, J.; Sanchez-Soto, M.; Velasco, J. I.; Santana, O. O. Ll, M.; MasPOCH, *Eng. Fail. Anal.* **2009**, *16*, 2604.